CHEMISTRY OF MATERIALS

ARTICLE

pubs.acs.org/cm

Effect of Strontium Substitution on the Structure of 45S5 Bioglasses

Ye Xiang and Jincheng Du*

Department of Materials Science and Engineering, Center for Advanced Scientific Computing and Modeling (CASCaM) University of North Texas, Denton, Texas 76203, United States

Supporting Information

ABSTRACT: Strontium substitution has been found to have a beneficial effect on tissue growth in traditional bioglasses. In this paper, we have studied the effect of SrO/CaO substitution on the structure of 45S5 bioglasses in the series of $46.1SiO_2 \cdot 24.4Na_2O \cdot (26.9-x)CaO \cdot 2.6P_2O_5 \cdot xSrO$ (x = 0, 1, 5, 10, 15) compositions using molecular dynamics (MD) simulations with effective partial charge potentials and a combination of constant temperature and pressure (NPT) and microcanomical (NVE) ensembles. The calculated neutron structure factor and neutron broadened total correlation function of the 45S5 glass were compared with experimental diffraction data and the two were found to be in reasonable agreement with each other. The SrO/CaO substitution effects on cation local environments were analyzed by studying the partial pair distribution functions, bond angle distributions, coordination number and its distribution. Change of the medium-range structures were characterized by Q^n distributions and network connectivity, cation−cation distributions and their aggregation, as well as the preference of modifiers around the glass former cations. It was found that strontium substitution leads to a linear increase of both molar volume and density. The Sr−O bond distance is found to be around 2.59 Å, and the average strontium coordination number is around 7.0 in the substitution series. The glass network structures such as Q^n distribution and network connectivity does not change much with SrO/CaO substitution. Calcium and strontium ions were found to preferentially distribute around phosphorus ions. These structural and property changes were correlated to observed glass dissolution behavior and bioactivity of strontium-containing bioactive glasses.

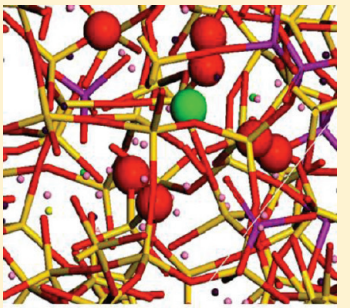

KEYWORDS: bioactive glass, glass structure, strontium substitution, clustering, structure factor, molecular dynamics simulation

1. INTRODUCTION

First introduced by Hench and co-workers, conventional bioglasses are basically sodium calcium phosphosilicate glasses that have the capacity to form intimate bonding to living tissues (soft and/or hard tissues in different compositions) through the formation of a hydroxylapatite layer at the glass/tissue interfaces. Because of their ability to promote tissue regeneration through gene activation and being absorbable in the body fluid environment, bioglasses can be classified as the third-generation bioactive materials, as compared to the first-generation bioinert materials and second-generation bioactive materials.[1] These glasses have been successfully used in a variety of biomedical applications ranging from bone graft extenders, bone defect filling materials, maxillofacial and periodontal treatment, to bioactive coating for metal implants and scaffolds for tissue engineering.[2]

After nearly four decades' study, the 45S5 bioglass is still considered to be one of the most bioactive compositions, and its structure and applications have been extensively explored. Recent efforts, however, have been shifting to prepare bioactive glass compositions with additional beneficial effects such as anti-inflammatory and bone growth enhancement. Strontium-containing glasses, in particular, have been actively studied due to the beneficial effect of bone growth introduced by strontium ions.[3] It is not coincident that strontium-containing drugs (e.g., strontium-containing Renelate) have been used clinically to treat osteoporosis.[4] An appropriate amount of strontium was found to promote osteoblast cell proliferation while inhibiting osteoclast cells to prevent bone resorption hence facilitate new bone growth.[5] Strontium-containing bioglasses thus provide enhanced bioactivity and tissue regeneration capabilities that can have potential applications in bone repair and substitution materials and in tissue engineering. The understanding of the strontium environment in the bioglasses, its effect on the glass network structure and glass dissolution, and the rate of strontium ion release in an aqueous environment is much needed in order to rationally design strontium-containing glass composition for biomedical applications. However, the atomic structure information and understanding of the structure−property relationship of Sr-containing bioactive glass are very limited. It is the purpose of this paper to apply molecular dynamics simulations to obtain detailed short- and medium-range structure information of strontium-containing bioglasses and to correlate them with important experimental observations such as the dissolution behavior of these glasses.

The effect of strontium on the structure and properties of apatite and several bioactive glasses has been studied experimentally. A substitution of slightly larger and heavier strontium to calcium was found to increase the unit cell volume and density in apatite.[6] Boyd and co-workers examined the structure of Na−Ca−Sr−Zn−Si oxide glasses using various methods to evaluate the effect of γ-irradiation on glass structure. The results

Received: October 6, 2010
Revised: April 18, 2011
Published: May 12, 2011

ACS Publications © 2011 American Chemical Society

showed no significant change in the local environment of silicon and the glass transition temperature due to irradiation.[7] Murphy et al. studied the ion release of strontium and zinc-containing soda lime silicate glasses as a vehicle for zinc and strontium ion delivery. It was found that increasing the Na_2O/ZnO ratio led to an increase of strontium release. A high level of zinc release was found at low pH values that led to a cytotoxic effect while strontium release was in a controlled manner in both low and high pH levels.[8] Meanwhile, there are contradictory results of the Sr/Ca substitution effect on the dissolution of glasses reported in the literature. For example, Lao et al. reported an evaluation of the in vitro reactivity of $SiO_2-CaO-SrO$ and $SiO_2-CaO-P_2O_5-SrO$ bioactive glasses derived from the sol−gel process. It was found that the transformation of bonelike apatite phase at the surface has a higher rate while the glass dissolution rate is reduced in strontium-containing glasses.[9] However, in the study of strontium-containing phosphate (Na_2O-CaO-P_2O_5) glasses, it was found that an addition of strontium accelerate glass degradation as well as dissolution.[10] O'Donnell and Hill pointed out in a recent review that the controversies on the effect of strontium on dissolution in the literature were introduced by the usage of weight percent, instead of the usual mole percent, during composition design in certain studies.[11] When substituted by weight percentage, the actual silica content in mole percent and thus the network connectivity is increased with the substitution of SrO/CaO, because of the higher molecular weight of SrO. The increase of network connectivity usually slows glass dissolution that counteracts the effect of strontium. The SrO/CaO substitution is generally believed to increase the dissolution of silicate glasses.[11]

Except for the extensive material and biological studies of bioactive glasses, there are considerable efforts to understand the structure of bioactive glasses through computer simulations and experimental structural studies due to the importance of the glass structure on the bioactivity of these materials. Neutron and X-ray diffraction experiments have been performed to study the 45S5 bioglasses (without strontium). Additionally, Reverse Monte Carlo (RMC) simulations based on the Neutron and X-ray diffraction results have been performed to extract structural information of the glasses.[12] The RMC modeling showed that the Ca−O bond length was 2.31 Å, and the coordination number of calcium was around 5. The Na−O bond length was 2.38 Å, and the coordination number of sodium was around 6. The structure from RMC modeling also suggested the existence of a certain level of clustering of modifiers.[12] At the same time, ^{29}Si NMR spectra were taken for 45S5 and the results show that the silica network consists of mostly chains and rings of Q^2 SiO_4tetrahedra with some degree of cross-linking by Q^3 units. The ^{31}P NMR spectra of the glasses proved the existence of isolated PO_4^{3-} anions but were not able to conclude on the existence of Si−O−P linkages.[12]

Tilocca and co-workers have studied the structure of bioactive glasses using molecular dynamics simulations.[13,14] Detailed structure information of bioactive glasses has been generated from these simulations that considerably advanced our understanding of the structure of these complex glasses. Both rigid ion and shell model classical molecular dynamics simulations have been employed.[15,16] Although both sets of potentials could generate reasonable bioglass structures,[13−16] utilization of the shell model to introduce the polarizability effect on oxygen ions was found to improve the description of certain structural aspects such as phosphorus Q^n distribution as compared to experimental data and the dynamic behavior in terms of silicon Q^n species transformation during the cooling process in comparison to the ab initio MD data.[16] phosphorus magic angle spinning NMR experiment of 45S5 bioglass suggested that majority of the phosphorus species should be Q^0, although small amount of Q^1 could also exist.[12] The 45S5 glass structure from shell model simulations had 82% Q^0 and 17% Q^1 for phosphorus, whereas the structure from rigid ion model had 47% Q^0, 42% Q^1 and 11% Q^2 species,[16] with both simulations using the same system size and a cooling rate of 10K/ps. Shell model simulations generated a much higher percentage of phosphorus Q^0 than rigid ion model simulations for 45S5 hence are in better agreement with experimental data. Even for the shell model simulations, there is room of improvement to further increase the percentage of Q^0 and decrease that of Q^1 phosphorus species in comparison to experimental results.[12,16] It was found that the increase of network connectivity, more P−O−Si linkages, and an aggregated calcium-phosphate-rich region were correlated to the decrease of bioactivity. It was also found that phosphorus has contradictory effect on bioactive silicate glasses. On one hand, the formation of P−O−Si linkage and modifiers' higher affinity around $[PO_4]$ than $[SiO_4]$ will reduce bioactivity; yet, on the other hand, the fast release of orthophosphate groups can boost bioactivity. Overall, the inclusion of phosphorus in small amounts had a positive effect on bioactivity,[17] as evident from the initial composition design of bioglasses. ab initio MD simulations of around one hundred atoms were also carried out to investigate the melt and glass structures. The final quenched glass structures are in reasonable agreement with those obtained by classical MD; this verifies the adequacy of classical MD to study glass structure and proves the reliability of MD to describe highly distorted environments in liquid.[18]

Pedone and co-workers have also provided a detailed study of the structure of bioactive glasses. Correlation of the structure moieties in the glass structure and properties has been made through quantitative structure activity relationship (QSAR) analysis. Recently, Pedone and co-workers studied the effect of magnesium oxide substitution on calcium oxide in bioglasses with the purpose of understanding the effect of substitution on mechanical properties.[19] The substitution of Mg brings a higher fraction of larger rings (10−12 members) and a lower amount of smaller rings (2 to 3 members), which leads to lower moduli of the glasses. In this study, $46.2SiO_2 \cdot 24.3Na_2O \cdot 16.9CaO \cdot 2.6P_2O \cdot 10MgO$ is found to be the best composition that has the lowest modulus and preserved bioactivity at the same time.

Because of the chemical similarity of strontium and calcium ions, such as ionic radius and charge, SrO/CaO substitution in bioactive glasses can be a strategy to develop new glass compositions with improved bone growth and regeneration capability while maintaining the general chemical and physical behavior of the base glass composition. In this paper, we study the SrO/CaO substitution effect in one of the most studied bioglass compositions−45S5−using molecular dynamics (MD) simulations. We have previously reported MD simulations of the structure of silica, sodium silicate and soda-lime silicate glasses using a set of effective partial charge pairwise potentials with very good transferability.[20−22] In this paper, we have carried out MD simulations using similar potentials with newly developed Sr−O potential parameters to understand the structural role of Sr and the effect of SrO/CaO substitution on the structure and properties of bioactive glasses based on the 45S5 composition. We will present the structures of these bioglasses in section 3 and discuss their relationship to properties of glass in section 4.

Table 1. Glass Composition, Final Simulation Cell Sizes, and Density

	composition (mol %)							
glass	SiO_2	Na_2O	CaO	P_2O_5	SrO	no. of Sr atoms	cell size (Å)[a]	density (g/cm^3)
45S5	46.1	24.4	26.9	2.6	0	0	33.81	2.649
S1	46.1	24.4	25.9	2.6	1	10	33.91	2.646
S5	46.1	24.4	21.9	2.6	5	50	33.97	2.712
S10	46.1	24.4	16.9	2.6	10	100	34.06	2.791
S15	46.1	24.4	11.9	2.6	15	150	34.24	2.845

[a] All simulation cells were in cubic shape. The sizes were for one side of the cube. Total number of atoms in the all simulation cells was 2835.

2. SIMULATION DETAILS

In Table 1, compositions and simulation cell information on the bioactive glasses in the series of $46.1SiO_2 \cdot 2.6P_2O_5 \cdot 24.4Na_2O \cdot (26.9-x)CaO \cdot xSrO$ (x = 0, 1, 5, 10, 15) are listed, where CaO is gradually substituted by SrO starting from the basic 45S5 Bioglass composition.

The conventional name 45S5 means that the weight percentage of SiO_2 is 45 and the atomic ratio of calcium to phosphorus is 5. The names of S1, S5, S10, and S15 represent different molar percentages of strontium substitution in the glass composition studied in our simulations. Each simulation cell contained 2836 atoms in a cubic box with an initial cell dimension to reproduce the experimental density of 45S5 glass (2.702 g/cm^3).[23] Larger simulation cells with 5672 atoms and smaller simulation cells with 1418 atoms have also been simulated for the 45S5 composition to study the simulation cell size effect. Related data and discussion on size effect are available in Supporting Information. All the results and discussion reported here are based on the simulation cell with 2836 particles.

The interatomic interactions were described by the Born model of solids using partial charge pairwise potentials. The covalent character of the bond is described by the partial charge on the ions. The short-range interactions have the Buckingham form $E_{ij}(r) = A_{ij}\exp(-r/\rho_{ij}) - C_{ij}/r^6$, in which r is interaction distance, A, ρ, C are parameters, the indices i and j stand for different atomic species. The partial charges and Buckingham potential parameters are listed in Table 2. The parameters were developed by cross fitting of the structure and physical properties of a large number of minerals. This set of potentials has been successfully applied to the simulation of silica, alkali silicate, aluminate, aluminosilicate, and phosphosilicate glasses, as well as for the bioglass compositions.[24,25] The efficacy and transferability of this set of potentials have been tested and verified by the study of a wide variety of multicomponent glass compositions.[20−22,24,25] Another advantage of the potential set is its efficiency in simulations that would allow the study of relatively larger simulation cells and long simulation time. The efficiency can also be of advantage in the simulation of dynamic behaviors that would involve long time simulations.

The total energy of the Buckingham potential has a maximum at low r and goes to negative infinity as r approaches zero. This character causes a problem at high temperatures during the glass formation process. Thus, a repulsive term was introduced to overcome this problem. The repulsion term, $V(r) = B/r^n + Dr$,[22] was adopted for r smaller than r_0, where r_0 was defined as the r value where the third derivative of potential energy approached zero. At r_0, B and n are chosen to make potential energy and their derivatives continuous.

Table 2. Atomic Charges and Buckingham Potential Parameters

pairs	A (eV)	ρ (Å)	C (eV Å^6)
$Si^{2.4}-O^{-1.2}$	13702.905	0.193817	54.681
$P^{3.0}-O^{-1.2}$	*26655.472*	*0.181968*	*86.856*
$O^{-1.2}-O^{-1.2}$	2029.2204	0.343645	192.58
$Na^{0.6}-O^{-1.2}$	4383.7555	0.243838	30.70
$Ca^{1.2}-O^{-1.2}$	7747.1834	0.252623	93.109
$Sr^{1.2}-O^{-1.2}$	14566.637	0.245015	81.773

All the potential parameters except for those for Sr−O listed in Table 2 have been used previously in modeling silicate and phosphate glasses and their validity and transferability have been extensively tested.[20−22] The Sr−O parameters were obtained by empirically fitting to the structure and physical property data of relevant crystals. A partial charge of 1.2 was assigned to Sr. Table 3 shows a comparison of the structure information calculated using this set of potential for strontium-containing crystals. The calculated lattice parameters of strontium oxide using the potentials were in good agreement with the experimental structure data and the difference of the lattice parameter and Sr−O bond length (2.566 Å) are within 0.1%. The potential sets were also able to reproduce more complex structures of $SrSiO_3$ and Sr_2SiO_4 with reasonable accuracy.

Molecular dynamics simulations were performed using the DL-POLY 2.20 program developed by Smith, Leslie and Forester at Daresbury Laboratory in the UK.[29] For the strontium-containing bioactive glasses, there is no experimental density data available in the literature. We chose to combine constant pressure, constant temperature (NPT) and constant volume−constant energy (NVE) MD simulations to generate the structure of these glasses following a simulated melt and quench process. The experimental density of the pure 45S5 composition served as a reference for the density of other glass compositions during simulation of these glasses.

The cutoff distance used for the short-range interaction was 8 Å. Long-range Columbic interactions were calculated using the Ewald sum method with a relative precision of 1×10^{-6} and a cutoff of 10 Å. Integration of motion equations was carried out using the Verlet Leapfrog algorithm with a time step of 1 femto second (fs).

The initial atom positions were generated randomly with the experimental density in a cubic simulation box. After initial relaxation at 300 K at zero pressure, the temperature was gradually increased to 4000 K through 1000, 2000, and 3000 K. At each temperature, we first ran NPT ensemble MD simulation for 60 000 steps (60 ps), which is then followed by an NVE run for another 60,000 steps. The glass was melted at 4000 K and then the temperature was gradually brought down to 300 K at a nominal cooling rate of about 5 K/ps. The total simulation time of each glass composition is around 14 ns. We also performed simulations with a cooling rate of 0.5 K/ps (total simulation time of 140 ns) to study the cooling rate effect on the structure for the S5 composition. (The effect of cooling rate on the structure of S5 can be found in the Supporting Information.) Equilibration at the melting temperature was confirmed by observing the average movement of each atom beyond half of the simulation cell size and a subsequent microcanonical (NVE) run without indication of large temperature fluctuation. The

dx.doi.org/10.1021/cm102889q |*Chem. Mater.* 2011, 23, 2703–2717

Table 3. Comparison between Calculated and Experimental Structures of Relevant Crystals Containing Strontium Using the Potential Parameters Listed in Table [2]

	SrO		$SrSiO_3$		Sr_2SiO_4	
	calcd	exp[26]	calcd	exp[27]	calcd	exp[28]
$a/b/c$ (Å)	5.132/5.132/5.132	5.156/5.156/5.156	12.154/7.066/11.199	12.333/7.146/10.855	5.759/7.107/10.919	5.679/7.078/11.040
$\alpha/\beta/\gamma$ (deg)	90./90./90.	90./90./90.	90./110.11/90.	90./111.57/90.	90./118.25/90.	90./117.01/90.
V (Å^3)	135.18	135.21	903.19	892.13	390.89	398.91
space group	*Fm*3*m*	*Fm*3*m*	*C*2/*c*	*C*2/*c*	$P2_1/c$	$P2_1/c$

Table 4. Cutoff Distances of First Coordination Shell for Coordination Calculations

pair	cutoff (Å)	pair	cutoff (Å)	pair	cutoff (Å)
Si−O	2.25	P−Ca	4.44	Na−Na	4.15
P−O	2.25	P−Na	4.44	Ca−Ca	4.85
Na−O	3.34	P−Sr	4.58	Sr−Sr	5.14
Ca−O	3.14	Si−Ca	4.37	Na−Sr	4.40
Sr−O	3.35	Si−Na	4.42	Ca−Sr	5.00
O−O	2.91	Si−Sr	4.51	Na−Ca	4.94

Nose−Hoover thermostat and barostat were used to control temperature and pressure during NPT MD simulations. At 300K, configurations of every 50 steps in the last 40 000 steps of the NVE run with a total of 801 configurations were recorded, based on which final structure analysis was carried out. We performed three independent MD simulations to generate three glasses for each composition. Each glass starts from distinct initial randomly generated configurations. The average structure data together with standard deviations over three structures were reported in tables. Error bars ae also provided in the figures.

Table 4 listed all the cutoff values used in following calculations such as bond angle distribution, coordination number and some clustering analysis. The cutoff values were obtained as the first minimum in corresponding partial correlation functions.

3. RESULTS

3. 1. Comparison with Experimental Diffraction Data. To validate the bioglass structure models we obtained from the MD simulations, we have calculated the neutron structure factors based on simulated glass structures and compared them with recent experimental data from neutron diffraction.[12] The partial structure factors were calculated by Fourier transformation of the partial pair distribution functions $g_{ij}(r)$ from MD simulations.

$$S_{ij}(Q) = 1 + \rho_o \int_0^R 4\pi r^2 [g_{ij}(r) - 1] \frac{\sin(Qr)}{Qr} \frac{\sin(\pi r/R)}{\pi r/R} dr \quad (1)$$

in which Q is the scattering vector, ρ_o is the average atom number density, and R is the maximum value of the integration in real space, which is set to half of the size of one side of the simulation cell. The Lortch type window function $\sin(\pi r/R)/(\pi r/R)$[30] was used during the Fourier transformation to reduce the effect of finite simulation cell size. The total neutron structure factor was

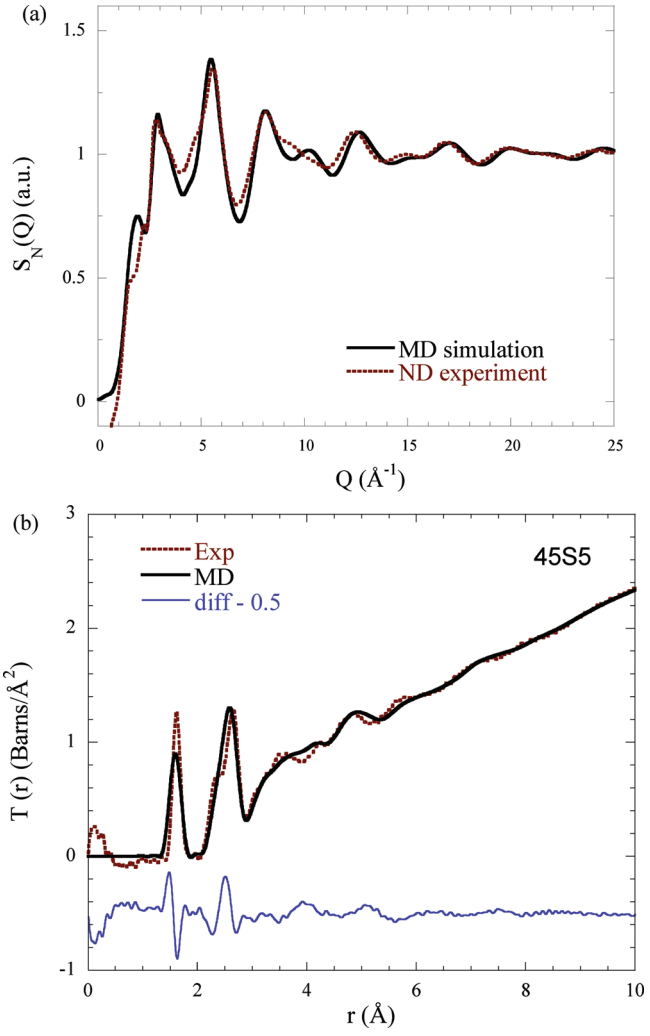

Figure 1. Comparison of (a) simulated and experimental[12] neutron structure factor and (b) neutron broadened total correlation function for 45S5.

then calculated by

$$S_N(Q) = \left(\sum_{i=1}^{n} c_i b_i\right)^{-2} \sum_{i,j=1}^{n} c_i c_j b_i b_j S_{ij}(Q) \quad (2)$$

in which c_i and c_j are the fraction of atoms and b_i and b^j are neutron scattering lengths, for element i and j, respectively. The neutron scattering lengths used are 5.803, 4.1491, 3.63, 4.70, 7.02, and 5.13 fm for oxygen, silicon, sodium, calcium, strontium, and phosphorus, respectively.[31]

Figure 1a shows the comparison of simulated and experimental neutron structure factor for 45S5. The calculated structure

dx.doi.org/10.1021/cm102889q |*Chem. Mater.* 2011, 23, 2703–2717

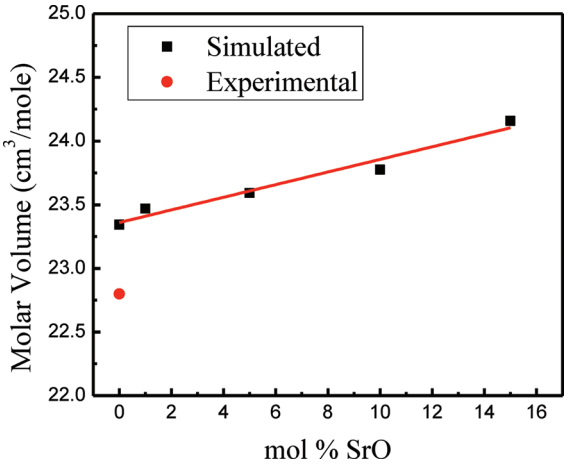

Figure 2. Calculated molar volume of the series $46.1SiO_2 \cdot 24.4Na_2O \cdot (26.9-x)CaO \cdot 2.6P_2O_5 \cdot xSrO$, where x = 0, 1, 5, 10, and 15.

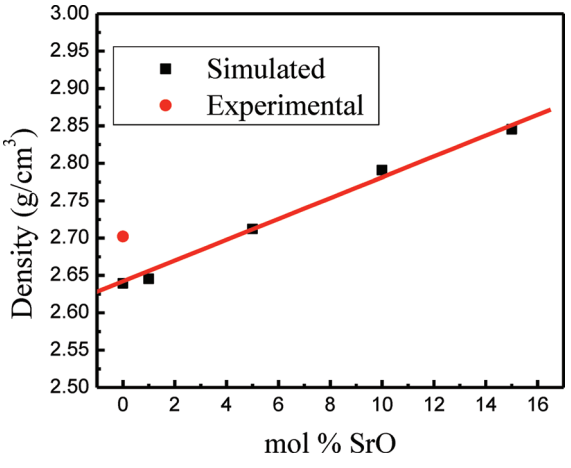

Figure 3. Calculated density of the series $46.1SiO_2 \cdot 24.4Na_2O \cdot (26.9-x)CaO \cdot 2.6P_2O_5 \cdot xSrO$, where x = 0, 1, 5, 10, and 15.

factor is in general good agreement with the experimental data, which indicates the atomic structure of 45S5 bioglass from our MD simulation provides reasonable structure models for the system. The largest difference was found to be at the first and the fifth peak. The calculated glass structure has a higher intensity of the first diffraction peak, while the experimental data only shows a shoulder, suggesting some differences in the medium-range structure. Otherwise the second, third and fourth peaks position and intensity are all in good agreement between the two sets of data. The features beyond 12 $Å^{-1}$ of the structure from simulations are also in excellent agreement with experimental data.

We also compared Figure 1b neutron broadened total correlation functions from the simulation with that obtained from Fourier transformation of the experimental structure factor of 45S5.[10] Again, the total correlation function from the simulation is in general good agreement with the experiment. The first and second peak positions agree well with the experiment. There are slight differences of the shapes of the peaks, as reflected from the difference curve. The experimental data has a shoulder on the lower r side of the second peak while that peak from the simulation seemed to be broader and more symmetric. Noticeable differences also exist on the third and fourth peak between the curves from the simulation and the experiment; the experimental data clearly shows two peaks, whereas that from the simulation shows a large broad peak.

The comparison in both reciprocal (structure factor) and real (total correlation function) spaces cross checked the structures of the generated 45S5 bioactive glasses using the current potential sets and simulation procedures. The general agreement between the experimental and the simulation data provided validation of our structure models. However, noticeable differences exist, especially the first peak in structure factor and the peak shape of the third and fourth peaks in the total correlation function, which point to directions of further improvement of future simulations, either from the potential models or simulation procedures.

3.2. Density and Molar Volume. The molar volume and density of the series of samples $(46.1SiO_2 \cdot 24.4Na_2O \cdot (26.9-x)CaO \cdot 2.6P_2O_5 \cdot xSrO$, x = 0, 5, 10, 15), which were calculated from the equilibrium cell volumes at 300K after constant pressure and constant energy MD simulations, are shown in Figure 2 and 3. Due to the larger size of Sr ions, the substitution of SrO for CaO results in a larger simulation cell volume and consequently large molar volume of the glasses. Meanwhile, Sr is heavier than Ca (with atomic weight of 87.62 and 40.078 g mol^{-1}, respectively) and therefore the weight of the cell also increases with the substitution of SrO in glass. The increase in cell weight dominates over increased cell volume, leading to a linear increase of density with SrO substitution (Figure 3). For 45S5, the calculated density is 2.639 g/cm^3, close to the experimental density of 2.702 g/cm^3. The theoretical density is around 2% lower than the experimental value. This difference is due to the fact that the potential parameters were not fitted to the amorphous systems but rather fitted to the relevant minerals. Although the potentials have been shown great transferability in multicomponent glasses, there is still a small difference of the predicted densities. Similar density differences in simulated glasses under constant pressure calculations were observed in other silica and silicate glass simulations.[21] The trend of density change with composition predicted by these simulations otherwise provides valuable information of the fundamental property change with strontium substitutions in these glasses from atomic level simulations. Mauro et al have correlated the equilibrium density of calcium aluminum silicate glasses from Monte Carlo simulations with experimental densities. The simulated densities, although slightly different in absolute value, were shown to correlate well and provide consistent trend of density change with composition as compared to the experiments.[32] Experimental densities of the strontium-containing bioglasses are not currently available in literature, thus a direct comparison is not possible at this moment. A linear increase in lattice parameters, cell volume and density was also observed in a series of strontium-substituted apatites $((Sr_xCa_{1-x})_5(PO_4)_3OH$, where x = 0.00, 0.25, 0.50, 0.75, and 1.00) using XRD and Rietveld refinement.[6]

3.3. Local Structure around Network Formers. The average coordination numbers of network formers, P and Si, are both four in all the compositions, with exceptions less than 0.1%. When considering partial contribution from BO and NBO, silicon, on average, has 2.1coordinated BO and 1.9 coordinated NBO while phosphorus is coordinated by 0.6 BO and 3.4 NBO in its first coordination shell. This result suggests that phosphorus is preferentially surrounded by NBO. Besides, the short-range structure is fixed over the change in composition when CaO is replaced by SrO. Further information about the P/Si—O

dx.doi.org/10.1021/cm102889q |*Chem. Mater.* 2011, 23, 2703–2717

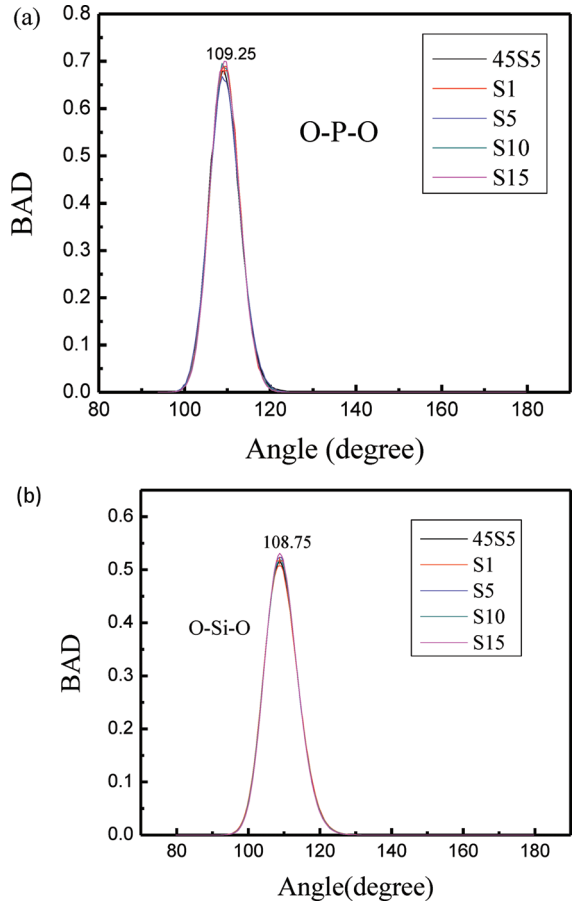

Figure 4. Bond angle distributions of (a) O−P−O and (b) O−Si−O in 45S5, S1, S5, S10, S15.

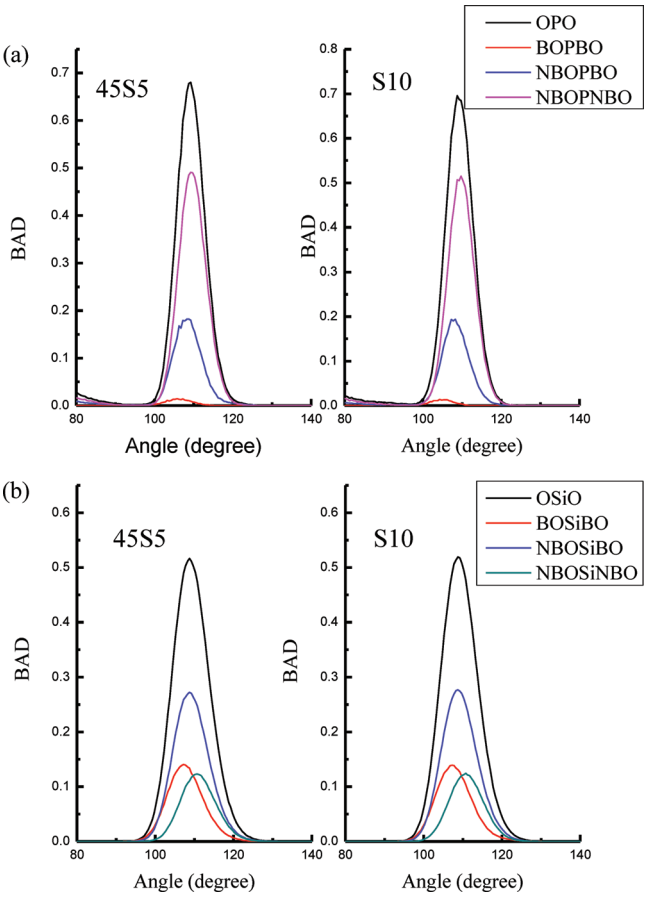

Figure 5. Total bond angle distributions and their BO/NBO contributions for (a) phosphorus and (b) silicon in 45S5 and S10.

coordination shell can be obtained from O−P−O and O−Si−O bond angle distribution (BAD) in Figure.4. The first peak position of O−P−O BAD is at 109.2° with a full width at half-maximum (fwhm) of 8.3°, whereas the peak of the O−Si−O BAD is at 108.8° with a fwhm of 11.1°. The O−P−O BAD is narrower and the peak position is closer to the optimal tetrahedral angle of 109.47°, due to the fact that P^{5+} has higher field strength and a higher number of NBO in coordination shell than Si^{4+}. The BAD results are in agreement with other simulation results: O−Si−O angle at 109.6 ± 7 and O−P−O at 109.7 ± 5.[18] Partial contributions of NBO and BO to the total O−Si/P−O bond angle distributions are illustrated in Figure 5. For Si, BO−Si−BO, BO−Si−NBO and NBO−Si−NBO play a role in total O−Si−O BAD, whereas the contribution from BO−P−BO is negligible, because Q^2 of P is limited (no more than 10% as shown in Table 6). The high NBO/BO ratio around phosphorus ions and associated large contribution of NBO in the intratetrahedral bond angle distributions in phosphorus supports the structural role of phosphorus in silicate glasses as a hunter of modifiers that repolymerize the silicate network.[33−35]

The connections between silicon oxygen tetrahedrons can be analyzed from Si−O−Si bond angle distribution (see Figure 6a). The results show the bond angle between [SiO_4] linkages is about 145° in 45S5 bioglass, similar to earlier simulation result[18] and Si−O−Si connection in sodium silicate glasses.[36] In experiment, the Si−O−Si BAD is also well studied using high-angle X-ray diffraction (HXRD), giving a distribution centered at 147° with fwhm of 35° for silica.[37] We can see from these results that 45S5 has a smaller Si−O−Si bond angle than that of silica of around 150°, which was simulated using the same potential sets. This trend agrees with previous results showed that introduction of modifier causes the decrease in Si−O−Si angle in the silicate network.[36]

The connection between phosphorus and silicon oxygen tetrahedron is represented by the Si−O−P bond angle distributions (see Figure 6b). Because of the relatively low number of such connections, as a result of low phosphorus concentration and higher percentage of Q^1 and Q^0 species, the intensity of the peak is considerably lower than that of the Si−O−Si bond angle distributions. The peak positions of Si−O−P BAD range from 150 to around 170° and with considerably larger fwhm than those of Si−O−Si BAD. The peak position at a larger bond angle is due to the fact that phosphorus has higher field strength due to its smaller size and higher charge that provide a stronger repulsion with silicon as compared to that between two silicon atoms in Si−O−Si linkages.

With the substitution of SrO, the local environment of silicon and phosphorus does not change. The coordination number of NBO and BO for P and Si remained the same. So on average, both Si and P are four-coordinated by oxygen. At the same time, the structure of [SiO_4] and [PO_4] tetrahedron and the connections between them do not show any changes. As for the bond angle distribution, a comparison between 45S5 and S10 in their partial contributions from BO and NBO is carried out, showing

dx.doi.org/10.1021/cm102889q |*Chem. Mater.* 2011, 23, 2703–2717

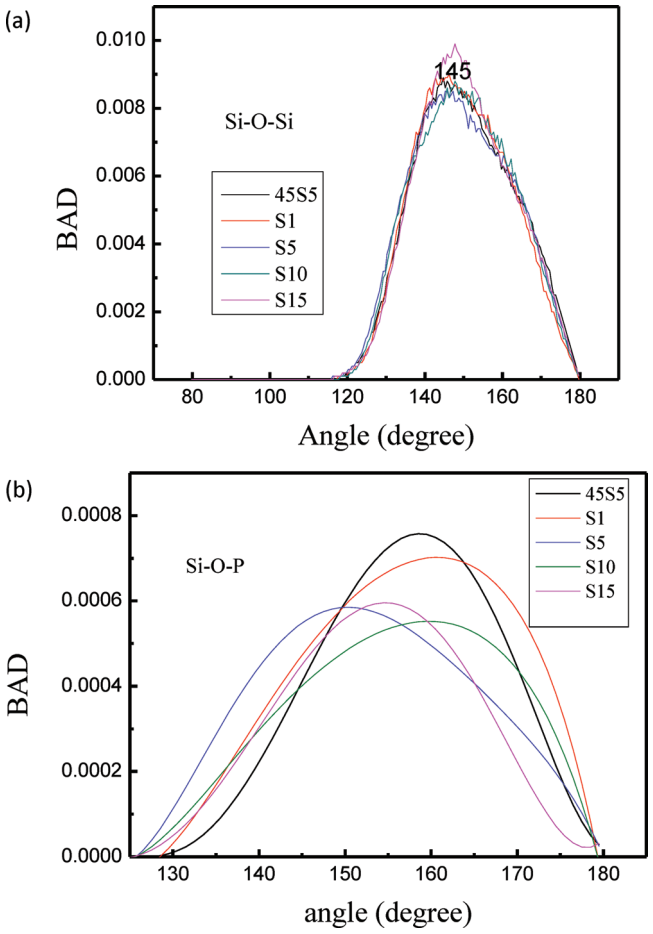

Figure 6. Bond angle distributions of (a) Si−O−Si and (b) Si−O−P in 45S5, S1, S5, S10, and S15.

no influence introduced by the 10 mol % SrO substitution. Thus, the total bond angle distribution remains the same for all samples, from 0 to 15 mol % substitution. Similarly, intertetrahedral bonding of Si−O−Si and Si−O−P does not change with replacement of CaO by SrO, shown in Figure 6.

3.4. Glass Forming Network Structure. Snapshots of network structure fragments including branched chains, ring structures, and isolated [PO_4] groups are shown in Figure 7. Analysis on Q^n, meaning n bridging oxygen ions per silicon or phosphorus tetrahedron, were performed in the simulated glasses to understand the glass forming network structures made up of [SiO_4] and [PO_4] tetrahedron. On the basis of the Q^n distribution, network connectivity (NC) can be calculated using $NC=\Sigma_{n=0}^{4} x_n n$ where x_n is the percentage of the Q^n (n = 0, 1, 2, 3, 4) species. The network connectivity for the two network formers, P and Si, and the average values are listed in Table 5. On the other hand, the theoretical network connectivity (1.90 for all studied compositions) was calculated based on the assumption that all Si and P ions were perfectly coordinated by four oxygen ions, each sodium ion generated one NBO, each calcium or strontium ion generated two NBOs, and each [PO_4] tetrahedron had one terminal oxygen.

According to our simulations (Table 6), silicon Q^n species are mainly in Q^2 (around 40%), whereas Q^1 and Q^3 also exist in large amount (around around 21.9−24.5% for Q^1 and 26.2−28.1% for Q^3). The trinomial distribution of Q^n for silicon

Table 5. Average network connectivity

	average network connectivity		
	Si (σ = ± 0.02)	P (σ = ± 0.03)	overall
45S5	2.07	0.62	1.92
S1	2.06	0.69	1.93
S5	2.09	0.59	1.93
S10	2.07	0.60	1.92
S15	2.09	0.52	1.93

in our simulation is supported by several other classical and Car−Parrinello molecular dynamics as well as Monte Carlo simulations.[19,23,38−40] Earlier experimental data suggested an ordered binary model containing only Q^2 and Q^3 species;[12,41] however, more recent Raman and NMR data indicated the trinomial distribution of Q^1 (∼15%), Q^2 (∼67%), and Q^3 (18%),[42−45] with the percentage of Q^2 species being higher than that predicted from MD simulations. There is also some controversy regarding the P Q^n distribution. In the experimental ^{31}P MAS NMR spectrum, one broad peak was assigned to isolated orthophosphate, strongly suggesting that majority of the P atoms, if not all of them, are present in the form of Q^0;[12,42] however, it is difficult to determine the exact amount of Q^1 due to limited resolution.[12] MD simulations have suggested considerable amount of Q^1 (around 33%) and some Q^2 (around 2%).[23] The results from our MD simulations also predict considerable amount of Q^1 and Q^2 species. More recent MD simulations with potentials that took oxygen polarization into consideration using the shell model have resulted in models with higher percentage of Q^0 species of around 82%.[16] The presence phosphorus Q^1 or Q^2 species has been suggested by other methods such as the features of P−O−Si bonds in FTIR in sol−gel derived bioglasses,[43] yet these features are present on the surface of the material only, and they are not stable when exposed to moisture in atmosphere.[44,45]

Within the whole spectrum of SrO/CaO substitution, for up to 15 mol % SrO, the distributions of Q^n species for both silicon and phosphorus remain essentially unchanged within statistical errors. As a consequence, the overall average network connectivity also remains around 1.9, very close to theoretical value of 1.90 of 45S5 glasses (assuming each strontium ion has the same effect as calcium to generate two NBOs).

3.5. Local Environment around Modifiers. *3.5.1. Bond Angle and Bond Length.* Partial correlation functions (T(r)) of Na−O and Ca−O in glass 45S5 and S10 are shown in Figure 8. The cation-oxygen bond lengths, which were obtained from the first peak position of the corresponding partial correlation functions, are listed in Table 7. The bond lengths for Na−O and Ca−O have similar values of 2.39 and 2.38 Å, respectively. The bond length from simulation is in good agreement with experiments: Wright et al. found the Na−O bond length to be around 2.36 Å based on neutron diffraction study of sodium silicate glasses.[44] Eckersley et al. studied the calcium environment in silicate glasses using neutron diffraction and it was found that the first peak in Ca−O pair distribution was well-defined, in agreement with what was found in our MD simulations. Additionally, the Ca−O bond length is around 2.37 Å, again in good agreement with our simulations.[46] Figure 8 also examines the substitution effect of SrO on bond length of sodium and calcium, showing no shift of peak position on the partial correlation functions. Therefore, it is safe to conclude that SrO/CaO

dx.doi.org/10.1021/cm102889q |*Chem. Mater.* 2011, 23, 2703–2717

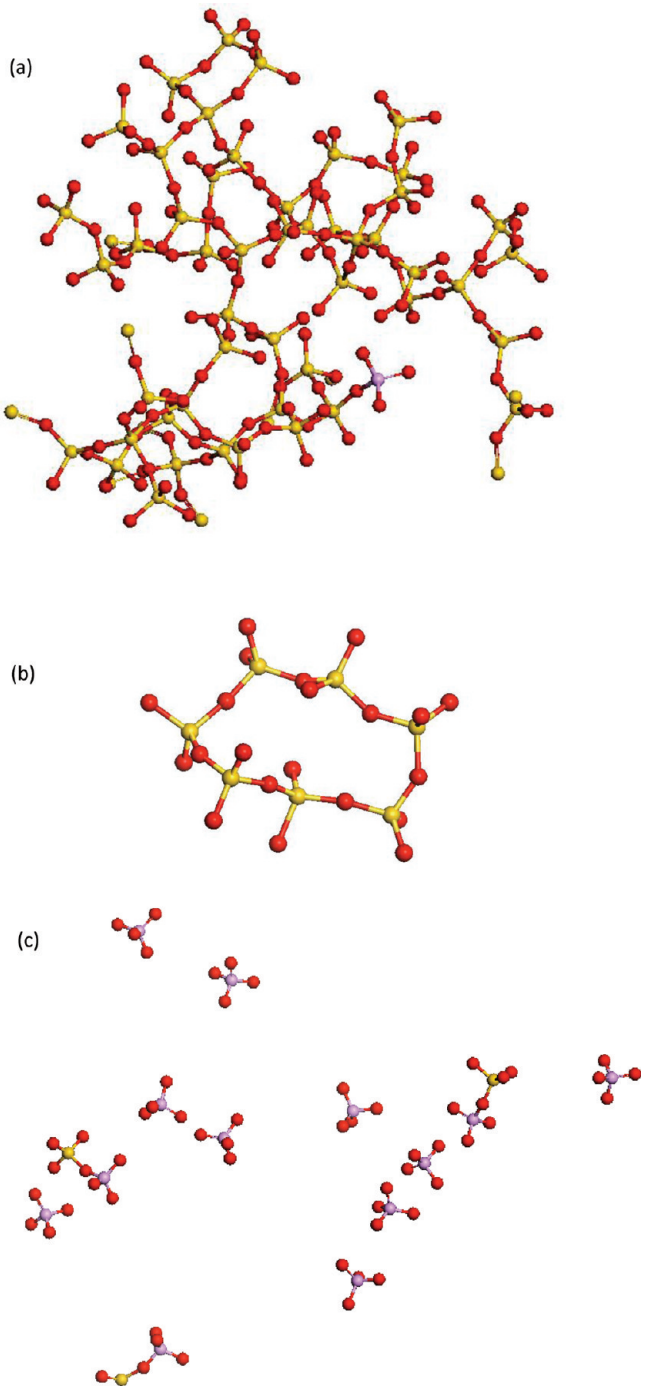

Figure 7. Snapshots of network structure fragments: (a) [SO_4] backbone; (b) short chain of [SiO_4] with a seven-member ring; (c) fragmented [PO_4] in 45S5. O, red ball; Si, yellow ball; P, purple ball.

substitution does not lead to changes in the average Na−O and Ca−O bond length.

Similar to calcium, the Sr−O first peak (Figure 8c) in partial correlation function is also symmetric and has high intensity, suggesting a well-defined first coordination shell. The Sr−O bond length from our simulations is around 2.59 Å and the coordination number of strontium is around 7.0, in general agreement with available experimental data. In an EXAFS study on strontium-containing borosilicate glasses, the Sr−O distance

Table 6. Q^n Species Distribution for P and Si

P	Q^0	Q^1	Q^2	Q^3	Q^4
45S5	50.0 ± 8.8	42.9 ± 7.8	6.4 ± 1.1	0.6 ± 1.1	0
S1	45.5 ± 2.9	47.3 ± 2.3	7.1 ± 4.0	0	0
S5	49.4 ± 4.4	43.0 ± 4.4	7.0 ± 1.1	0	0
S10	47.4 ± 2.9	46.8 ± 5.9	5.8 ± 3.3	0	0
S15	53.8 ± 10.2	41.0 ± 10.6	2.6 ± 1.1	1.3 ± 2.1	0
Si	Q^0	Q^1	Q^2	Q^3	Q^4
45S5	3.7 ± 0.4	23.2 ± 1.6	39.8 ± 1.4	27.8 ± 2.0	5.6 ± 1.3
S1	3.8 ± 1.1	21.0 ± 1.3	42.9 ± 0.9	27.8 ± 1.9	4.6 ± 0.8
S5	3.0 ± 0	22.0 ± 1.4	42.4 ± 2.2	28.2 ± 1.1	4.4 ± 0.1
S10	3.5 ± 1.1	23.2 ± 0.9	41.1 ± 2.6	25.9 ± 1.5	6.3 ± 0.9
S15	3.1 ± 0.8	21.5 ± 1.2	42.1 ± 2.2	29.1 ± 1.1	4.2 ± 0.7

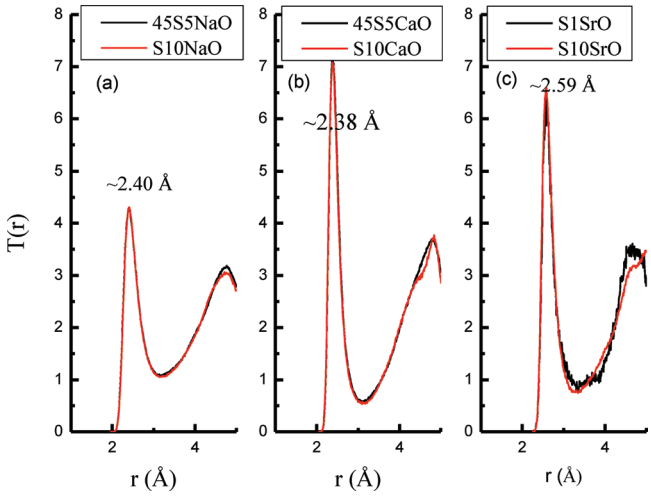

Figure 8. Partial correlation functions (T(r)) of (a) Na−O, (b) Ca−O, and (c) Sr−O.

Table 7. Bond Lengths (Å) of the Simulated Glasses and Those from Experimental Study (standard deviation for bond Length is 0.01 Å)

	45S5						
pairs	our MD	core−shell MD[a]	RMC[b]	S1	S5	S10	S15
O−O	2.63	2.64	2.64	2.63	2.63	2.63	2.64
Si−O	1.61	1.59	1.61	1.61	1.61	1.61	1.61
Ca−O	2.38	2.29	2.31/2.59	2.38	2.39	2.39	2.39
Na−O	2.40		2.35	2.4	2.4	2.4	2.4
Sr−O				2.59	2.55	2.57	2.58
Si−Si	3.16		3.03	3.16	3.17	3.16	3.16
Si−Na	3.29		2.96	3.28	3.33	3.27	3.28
Si−Ca	3.64		3.25	3.6	3.62	3.6	3.61

[a] Core−shell model molecular dynamics results from ref 23. [b] Reverse Monte Carlo Modeling based on Neutron and X-ray Diffraction Study in ref 12.

was found to be 2.52 Å and coordination number was reported to be 4.0−5.0.[47] Another study in tin silicate glasses using neutron and X-ray diffraction revealed a transition of strontium

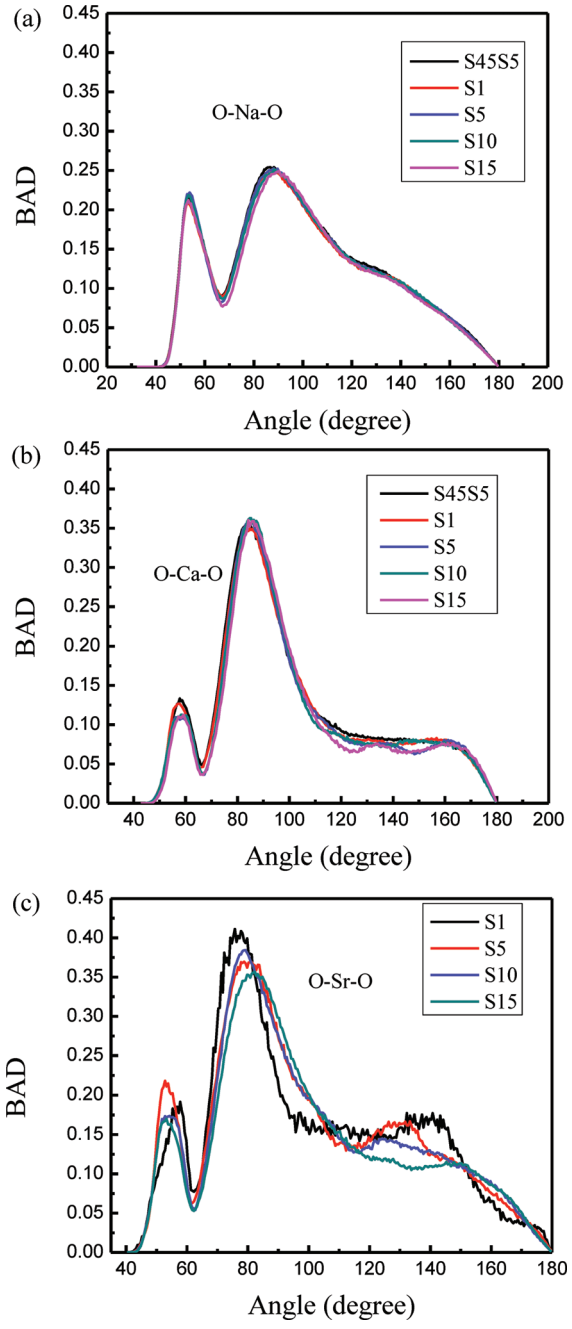

Figure 9. Bond angle distributions of (a) O−Na−O, (b) O−Ca−O, (c) O−Sr−O.

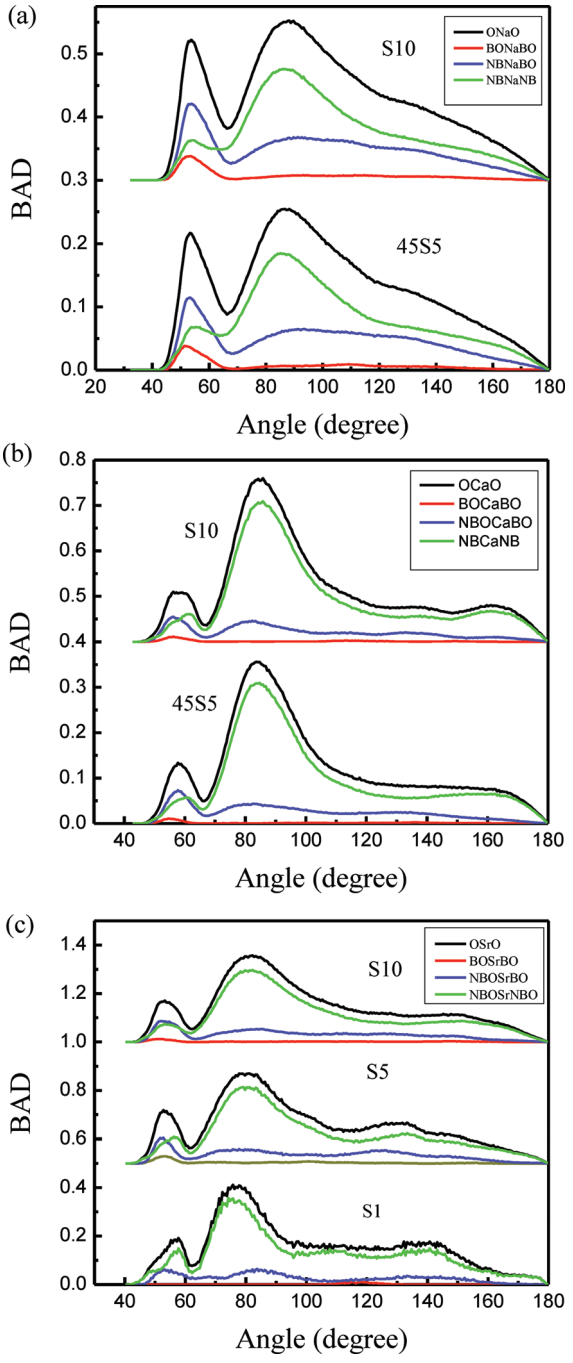

Figure 10. Comparison of bond angle distributions and NBO/BO contributions for 45S5 and S10 for (a) O−Na−O, (b) O−Ca−O, and (c) O−Sr−O.

environment in tin silicate glasses: the Sr−O distance undergoes a step decrease from 2.640 Å to 2.585 Å as x increase from 0.10 to 0.15 in $(SrO)_x(SnO)_{0.5-x}(SiO2)_{0.5}$,the corresponding coordination number of strontium decreased from 8.0 to 7.0.[48]

The total O−Na−O, O−Ca−O bond angle distributions for all the calculated samples are shown in Figure 9, based on the listed cutoff values in Table 4. Both the O−Na−O and O−Ca−O distribution extends from 40 to 180° with two main peaks at around 60 and 90°, in agreement with classical molecular dynamic simulations by rigid ion or core−shell potential.[16] Yet, the intensity of two peaks is close to each other for Na, whereas the intensity of peak at 60° is much weaker than that at 90° in the case of O−Ca−O. An explanation is available from information obtained from partitioned BAD shown in Figure 10. The peak at 90°, results from the octahedral geometry connecting two NBO from different $[SiO_4]$ or $[PO_4]$. Thus, the higher proportion of NBO in the first coordination shell of calcium explains the dominance of this peak in the O−Ca−O distribution. On the other hand, the O−Na/Ca−O bond angle at 60° forms only when the sodium or calcium ions are coordinated to the oxygen ions belonging to the same tetrahedron. This geometrical environment requirement is easier satisfied by sodium, because of its smaller radius, and therefore the intensity of peak of 60° is relatively high for Na than Ca. As discussed above, average

dx.doi.org/10.1021/cm102889q |*Chem. Mater.* 2011, 23, 2703–2717

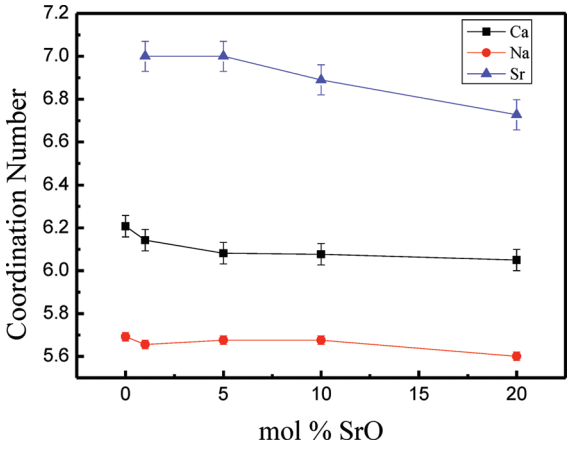

Figure 11. Average modifier-oxygen coordination number.

Na−O and Ca−O bond length is independent of the level of SrO/CaO substitution. Here, in the case of bond angle, no shifts were found in peaks of BAD in Figure 9 and their contributions from bridging oxygen and nonoxygen remained the same when comparing 45S5 and S10. Therefore, O−Na−O and O−Ca−O bond angle distributions are not sensitive to the level of SrO/CaO substitution.

The O−Sr−O bond angle distribution has two main peaks with different intensities: the strongest at around 80°and the secondary strongest at about 50°. Figure 9c shows partitioned BAD plot of O−Sr−O, revealing contributions from BO−Sr−BO, BO−Sr−NBO, and NBO−Sr−NBO to the total O−Sr−O bond angle distribution. O−Sr−O bond angle distribution is dominated by NBO−Sr−NBO at around 80°, whereas the other peak at about 55° is mainly contributed by both NBO−Sr−NBO and NBO−Sr−BO; yet, BO−Sr−BO contributes little to either. In both the TDF and BAD plots, Sr has similar features to Ca than to Na, which proves the functional resemblance between calcium and sodium in glass structure and hence bioactivity.

3.5.2. Modifier Coordination Numbers. The average coordination numbers (CN) for all modifiers are shown in Figure 11 and their distribution is provided in Figure 12. In the 45S5 glass with no substitution, the coordination number of Ca ranges from 4 to 9, most of which are 5, 6, and 7, resulting in an average coordination number of 6.2. Compared to Ca, Na has a broader distribution and slightly lower average CN of around 5.7. These results are in in good agreement with previous simulation work, which found the coordination number of Na and Ca being 5.6 and 6.2, respectively.[16] As for substituted samples S1 to S15, four- and five-coordinated calcium increase, whereas seven- and eight-coordinated calcium decrease. Majority of calcium ions are six-coordinated and the percentage of the six-coordinated calcium increase with the substitution. The average calcium coordination number, however, drops slightly from 6.2 of 45S5 to 6.0 of S15. Similarly, the substitution of Sr for Ca leads to a slight decrease of Na coordination number, which is mainly due to the decrease of six-coordinated Na and the increase in five-coordinated Na.

Strontium has an average coordination number of 7.0 (a strontium−oxygen coordination polyhedron is shown in Figure 13. As SrO concentration increases, the strontium coordination number distribution becomes narrower, consistent with the observed O−Sr−O BAD changes. The percentage of 6- and 7-coordinated strontium grows while that of 5-, 8-, and

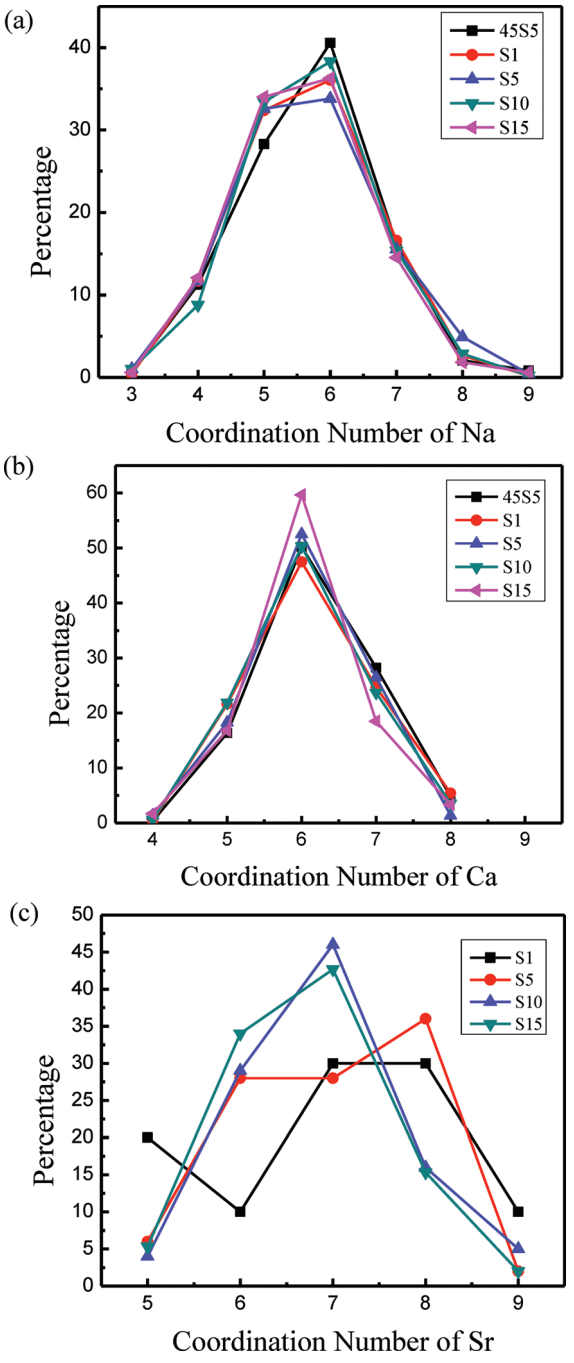

Figure 12. Oxygen coordination number distributions for modifiers (a) sodium, (b) calcium, and (c) strontium.

9-coordinatd strontium decreases. Overall the coordination number of Sr decreases slightly with SrO substitution. Because of larger ionic radii and thus weaker field strength of Sr^{2+}, the distribution of coordination number for Sr is generally broader than that of Ca.

The BO and NBO contributions in the first coordination shell of the modifiers depend strongly on the types of the modifiers. In the series of these glasses, the percentage of nonbridging oxygen ions is close to 68%. As shown in Figure 14, in the first coordination shell of modifiers, the percentage of NBO in total oxygen is larger than 68% (90% for Ca, 88% for Sr, and 80% for Na). Therefore, all three modifiers have preference of NBO in

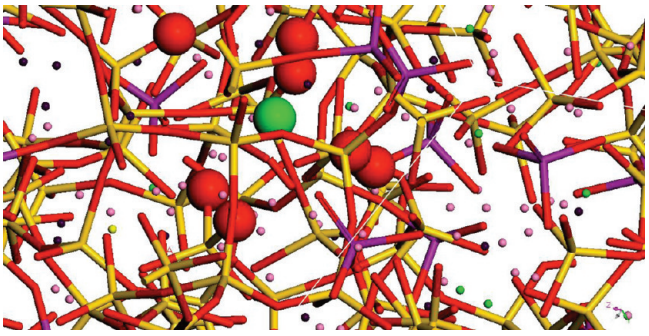

Figure 13. Snapshot of strontium environment in 45S5 bioglass. First coordination shell of oxygen (red) around strontium (green) was shown in large balls. Modifier cations: Sr, green ball; Na, pink ball; Ca, purple ball. Network: silicon, yellow bar; P, purple bar; oxygen, red bar.

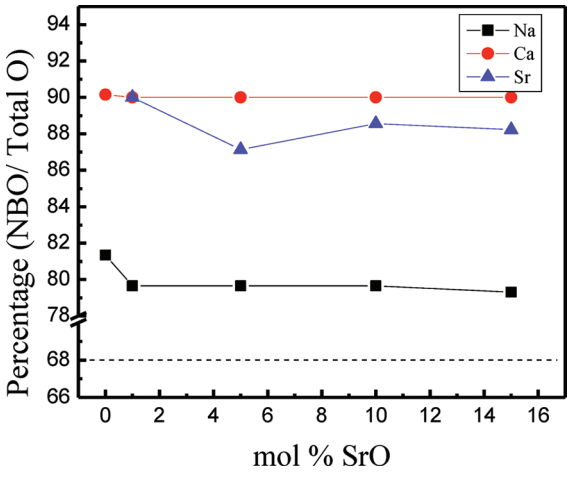

Figure 14. Percentage of NBO in modifier-oxygen coordination shell; dotted line: percentage of NBO over total oxygen ions.

their first coordination shell. However, the preference is the strongest for Ca and weakest for Na, which can be explained by the sequence of field strength which decreases in the series of Ca^{2+}, Sr^{2+}, and Na^{1+}. (Modifier field strengths are 0.36 for Ca, 0.30 for Sr, and 0.18 for Na. The field strengths were calculated from size ratio Z/r^2, in which Z is cationic charge and r is cation-oxygen interionic distance. The interionic distance was calculated based on the Shannon ionic radii[49] using the calculated average cation coordination number from simulation).

3.6. Modifier Distribution and Microheterogeneity in the Glass Structure. The medium-range structures are very important in the dissolution process and thus bioactivities of the bioactive glasses. In the modified random network model of silicate glasses, it has been suggested that there exist modifier rich regions and network former rich regions. The microsegregations of modifiers, NBO, and network formers have strong influence on the glass properties including the dissolution behavior. By using a number of characterization methods, we here examine the effect of SrO/CaO substitution on the distribution of modifiers and segregation of ions, especially the modifier cations, in strontium-substituted 45S5 bioactive glasses.

3.6.1. Coordination Number of Modifiers around Network Formers. The Si/P-modifiers (Na+Ca+Sr) pair distribution functions (PDF) of 45S5 and S10 are shown in Figure 15. For both phosphorus and silicon, there exists a fairly well-defined first

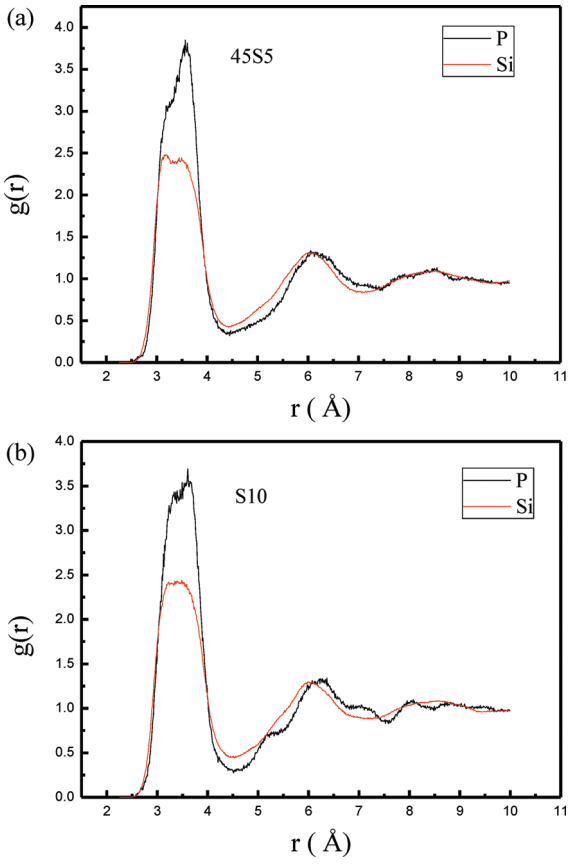

Figure 15. Si-all modifiers and P-all modifiers pair distribution functions (PDF) in 45S5 (a) and S10 (b).

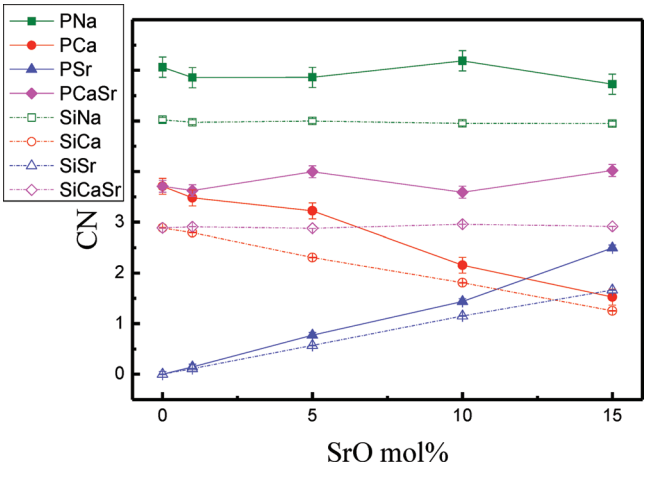

Figure 16. Coordination numbers of modifiers around network formers.

peak at around 3.6 Å. However, the P-modifier first peak intensity is larger than that of Si-modifier, which indicates that the probability of phosphorus ions to be surrounded by modifiers is much higher than silicon, which further support that phosphorus ions are preferentially surrounded by modifiers that in turn polymerize the silicon−oxygen network. The coordination environment of modifiers around P and Si is illustrated in Figure 16: coordination number (CN) was calculated by

dx.doi.org/10.1021/cm102889q |*Chem. Mater.* 2011, 23, 2703–2717

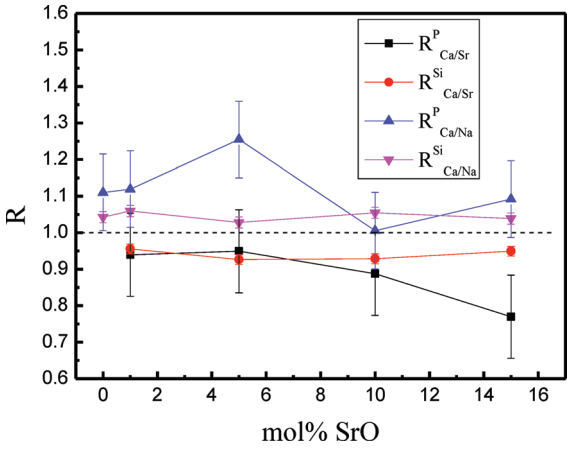

Figure 17. $R^{A}_{B/C}$ ratios for silicon and phosphorus.

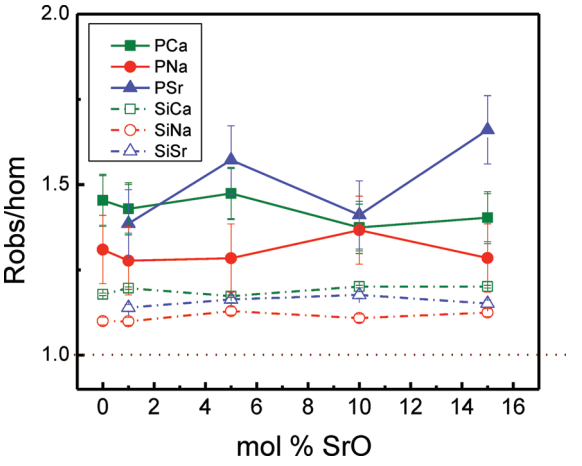

Figure 18. R^{obs}_{hom} ratios for modifiers around network formers.

integrating T(r) plots until the first minimum listed as cutoff in Table 4. At the composition of 45S5, shown in figure, the coordination number of Na around Si and P is five and six, separately. Meanwhile, Si is surrounded by three Ca ions and P is surrounded by four. It indicates that phosphorus ions are preferentially surrounded by modifiers that in turn polymerize the silicon−oxygen network. When CaO is increasingly substituted by SrO, the coordination number of sodium around both phosphorus and silicon remains unchanged. The coordination number of calcium shows a linear decrease and that of strontium increases, both around P and Si. The CN of Sr and Ca around glass former cations change linearly and are proportional to the number of Sr and Ca ions present in the simulation box. Thus, when we calculated the sum coordination number of Sr and Ca, with the total number of Ca and Na ions in simulation cell constant for all compositions, P is constantly coordinated by four and Si is coordinated by three, suggesting similar structural role of strontium and calcium during the substitution. As a result, taking all modifier species into consideration, including sodium, calcium and strontium, the CN of silicon is around eight and phosphorus has a CN of ten. Consistent with the stronger peak in phosphorus-modifier pair distribution function (Figure 15), the larger CN of modifiers around P, again, reflect phosphorus's ability to attract modifiers to its vicinity in silicate glasses and its effect to repolymerize Si−O network. Such ability is neither enhanced nor decreased by the SrO/CaO substitution in bioglass.

3.6.2. Preferential Distribution and Aggregation of Cations. The preference for specific modifiers around glass former cations can be characterized by calculating the ratio R[23]

$$R^{A}_{B/C} = \frac{CN_{A-B}}{CN_{A-C}} \times \frac{N_C}{N_B}$$

where A stands for the network formers, P or Si; and B, C mean two different types of modifier cations among Na, Ca or Sr; N_B is the number of B type of cation present. When the ratio R is near to one, B and C ions distribute around A statistically, according to their number density in the cell, in which case A performs no preference for B over C, or vice versa. Yet, a ratio of R >1 suggests the preference for B, whereas a ratio less than 1 denotes the affinity of C. As the values of R shown in Figure 17, compared with Ca, both phosphorus and silicon prefer Sr to Ca in their first coordination shell in all compositions; meanwhile, the glass formers prefer Ca to Na in all glasses from 45S5 to S15. The glass formers' preference for modifiers is consistent with the trend of modifiers' coordination number in Figure 11 and analysis above in section 3.5.2. The larger coordination number of Sr (7.0) than Ca (6.2) and Na (5.6) demonstrates a stronger ability of Sr to attract oxygen from the network of P and Si, so in the coordination shell composed by modifiers, Sr is the most preferred, followed by Ca and Na.

Except for coordination number and preference for different modifiers, the distribution of modifiers, homogeneous or clustered, tells us important information about the medium-range glass structure and the tendency of ion segregation. Here we use the ratio between observed coordination (CN_{obs}) and theoretical coordination number in the case of homogeneous distribution (CN_{hom}) to characterize the clustering behavior. In the definition, $R^{obs}_{hom} = CN_{obs}/CN_{hom}$, CN_{obs} is the observed coordination number shown in Figure 11 and $CN_{hom} = (4\pi/3)r^3\rho_0$, in which ρ_0 is the number density of coordinating ions while r is the same cutoff used in CN_{obs} as listed in Table 4. Similar methodology has been used to study calcium clustering in calcium silicate glasses[50] and bioglasses.[23] As a result, a R^{obs}_{hom} value much larger than 1 suggests that there exist a tendency of segregation while a homogeneous distribution of modifiers gives a R^{obs}_{hom} value close to 1. For different network formers, phosphorus and silicon, the tendency of ion aggregation has distinctive trends as reflected by the R values (Figure 18). With R^{obs}_{hom} values >1, all the modifiers, sodium, calcium, and strontium, have a tendency of clustering around phosphorus and this segregation tendency of around Si and P does not systematically increase or decrease with the SrO/CaO substitution. Compared to sodium, calcium, and strontium have a stronger segregation tendency as shown by their larger R value. Similar segregations have been observed in simulations of related systems: the microsegregation zone of calcium phosphate was found in phosphosilicate glasses due to the calcium−phosphorus affinity.[51] Considering the similar chemical nature and thus similar structural role of Sr and Ca in the glasses, it is thus expected that Sr and Ca has similar trend of clustering around P. And the trend of clustering is fairly insensitive to the changes of SrO/CaO concentration, as shown in Figure 18. For silicon, both the R^{obs}_{hom} values are close to 1, indicating no clustering of modifiers around them. The distinction between silicon and phosphorus is consistent with results presented earlier: the higher coordination number of sodium and calcium around phosphorus than silicon (Figure 16) and higher intensity

in peaks of P-modifier pair distribution functions than silicon (Figure 15).

4. DISCUSSION

Experimental investigations of strontium-containing oxide glasses revealed that Sr−O bond length and coordination number vary in different glass systems. In borosilicate glasses, EXAFS study showed an average Sr−O distance of 2.53 Å and a coordination number of 4.0−5.0,[47] while in sodium silicate glass AWAXS study revealed a Sr−O distance of 2.73 Å.[52] In aluminosilicate glasses, the Sr−O distance was found to be 2.68 Å and the coordination number to be around 6.0.[52] Neutron and X-ray diffraction studies of strontium-containing tin silicate glasses showed that the Sr−O bond length undergoes a step decrease from 2.64 to 2.58 Å as SrO concentration increases, with a corresponding decrease in coordination number from 8.0 to7.0.[48] Our simulations showed that strontium ions have a Sr−O bond length of 2.59 Å and a coordination number of 7.0 in strontium substituted 45S5 bioglasses. The Sr−O bond length and strontium coordination numbers of substituted 45S5 glasses from simulations are in good agreement with those in tin silicate glasses. In addition, we also observed a slight decrease of strontium coordination number from around 7.0 to 6.7 as SrO concentration increases from 1 to 15 mol %, similar to what found in the tin silicate glasses from diffraction studies.[48]

The short-range structural features of both network formers and network modifiers (coordination number, bond length and bond angle) do not change much with the SrO/CaO substitution. A slight decrease of strontium and calcium coordination number with SrO concentration was observed. The network structure also seemed to be insensitive to the substitution. This can be revealed by the small variations, mostly within statistical errors, of Q^n distributions, for both silicon and phosphorus, and the average network connectivity with the level of substitution. The close similarity of the theoretical network connectivity and that from simulations revealed that strontium ions act as glass network modifiers and play similar structural role as calcium ions in phosphosilicate glasses.

Phosphorus plays an intriguing role in the network structure of strontium substituted 45S5 glasses. Phosphorus can be considered to be a modifier scavenger, with the net effect being to increase the network connectivity of silicon. There are about 50% of phosphorus oxygen tetrahedra are Q^2 and Q^1 species in the 45S5 glass series. The phosphorus ions in these Q^n species participate in the glass network structure, either in the middle (Q^2) or at the end (Q^1) of the chains. Because of the much higher reactivity with water of phosphorus groups,[53,54] their distribution will play an important role in the dissolution process and thus the bioactivity of bioactive glasses. The presence of Q^1 and Q^2 phosphorus species will facilitate the dissolution of the silicon oxygen network since they are the weakest link in the chain or ring structures when in contact with the aqueous environment. Detailed discussion on the structural role of phosphorus in bioactive glass is available in ref 17.

There is still controversy in the literature on the exact amount of Q^0 species in 45S5 and similar bioglasses. NMR studies of phosphorus revealed one peak suggesting mostly Q^0 species of phosphorus in 45S5.[12] However, it could not rule out the existence of Q^1 or even Q^2 species and the Si−O−P linkage because of the limited sensitivity of the NMR method. In simulated glass structures, the percentage of Q^0 species of phosphorus depends on the potential models used and, very importantly but not fully understood, on the thermal history during the glass formation. Simulations using shell models to take into consideration of ion polarizability seemed to generate structure models with a higher percentage of Q^0 species of around 65%.[23] We have performed MD simulations of the 45S5 glass with 5 mol % SrO/CaO substitutions with two cooling rates: one is 5 K/ps and one is 0.5 K/ps. In the literature, MD simulations of glasses usually use a cooling rate of 1−10 K/ps. The 5Sr bioglasses generated in this work with two different cooling rates show similarity in most structural aspects such as local environments of cations, and silicon Q^n distributions. The calculated structure factors were also very similar between the two glasses generated with the slower and regular cooling rate. However, surprisingly, it was found that the phosphorus Q^n distributions are very sensitive to the cooling rate. With a slower cooling rate, the percentage of Q^0 increased from 45% for 5 K/ps to 75% for 0.5 K/ps cooling rate (see details in the Supporting Information). Due to the importance of phosphorus Q^n species on bioactivity, the sensitivity of phosphorus Q^n species with the cooling rate suggests that the dissolution behavior and the bioactivity are also different for the two glasses. This suggests that we can change the dissolution and bioactivity of these glasses by changing cooling rate or the thermal history during glass formation. This is yet to be proved by experimental studies.

Structure heterogeneity of multicomponent glasses plays an important role in the physical and chemical properties. With the glass former concentration being lower than 50 mol %, 45S5 can be classified as an invert glass, in which the glass modifier concentration is higher than 50%. With most of the network structure being chains, branched chains or small rings, the glass structure is highly fragmented. Determining the spatial distribution of the modifier cations can be a way of characterizing the heterogeneity of the glass structure. We have studied the modifier cation and glass former cation distribution and correlation factors. It was found that phosphorus and Ca/Sr ions are preferentially clustered. The preferential coordination of Ca/Sr around phosphorus ions and thus the fact that phosphorus ions are mainly in Q^0 and Q^1 species can lead to a weakening of the Si−O network. This is because as compared to sodium, calcium and similarly strontium ions have higher field strength that can provide stronger bonding among fragments of silicon−oxygen network as evidenced in much higher chemical durability of soda lime silicate glass as compared to soda silicate glasses with similar silica content.

Network connectivity of glasses has been used as a convenient quantitative measure of the bioactivity and reactivity.[55] Glasses with network connectivity below 2, demonstrating the network structure close to a two-dimensional chain structure, are usually required for a glass to be bioactive. It was indeed found experimentally that the bioactivity undergoes a dramatic change when the glass composition has network connectivity close to 2.[11] Except network connectivity, other aspects that can change the local chemical environment and reaction behaviors can also influence the bioactivity and the dissolution behavior. One of these aspects is the field strength of modifier cations. For example, calcium ions have a very different effect on the physical property and chemical durability in silicate glasses than sodium ions. With higher field strength, calcium ions can bond the network structure pieces together and improve the mechanical strength and chemical durability of sodium silicate glasses. The dissolution behavior can also be influenced by the field strength

of modifier cations. In binary series of alkali earth metasilicate glasses, even with no changes in network connectivity, dissolution rates will increase in the sequence of $SiO_2-MgO < SiO_2-CaO < SiO_2-Na_2O$,[11] following the sequence of decreasing field strength of modifiers. Therefore, when CaO is substituted by SrO in 45S5 bioglasses, since strontium has a larger radius and hence a lower field strength, we can expect an increase in ionic dissolution rate. The increase of molar volume with increasing SrO/CaO substitution can also contribute to the change of diffusivity of ionic species and thus the ion exchange process that lead to a higher dissolution rate. This is in agreement with experimental observations that, when substituted based on mole percentage, strontium substitution leads to a higher dissolution rate of bioglasses.[11]

Indeed, strontium is a natural component in human bone and strontium containing drugs has been used as oral intake to treat osteoporosis. Although the exact biological origin is still unclear, research on the biological role of Sr found that strontium Renelate, in low doses, can increase bone mass and bone strength while decreasing the chance of fracture, through inhibiting the resorption of bone, and at the same time, increase bone formation and the number of bone-forming sites. It has also been found that the usage of Sr at a high level will result in bone change, especially when intake of Ca is limited.[5] Thus, taking into considerations the change of dissolution rate due to SrO/CaO substitution and the harmful effect on bone change due to release of large amount of strontium ions, SrO concentration should be less than 5 mol % in strontium containing bioactive glasses that can serve as novel biomaterial with high bioactivity for bone regeneration. Strontium containing bioactive glasses and related biomaterials such as hydroxylapatite can also be used as bone grafting materials that combine the bioactivity and biocompatibility and the beneficial effect of bone growth due to strontium, they can also be used as bioactive coatings for metal implants. In addition, these materials can act as strontium delivery agent to release strontium ions to the surrounding tissue in a controlled way.

5. CONCLUSIONS

Constant pressure molecular dynamics simulations have been applied to the study on the structure of strontium substituted 45S5 bioactive glasses $46SiO_2-24.4Na_2O-(26.9-x)CaO-2.6P_2O_5-xSrO$ ($x = 0, 1, 5, 10, 15$), using a set of effective partial charge potentials. It is found that both molar volume and density of the series of glasses increase linearly with respect to the amount of SrO substitution. Detailed structural information on strontium environment in 45S5 glass was obtained and the results show Sr−O has a coordination number of 7.0 and a bond length of about 2.59 Å. Majority of the oxygen ions in the first coordination shell of calcium, strontium and sodium ions are nonbridging oxygen ions and the coordination number decreases slightly with increasing SrO concentration. The SrO/CaO substitution has little effect on the glass network structure, as indicated in the Q^n distribution and average network connectivity. The local environments of other modifiers such as sodium and calcium were also found not to be affected by the substitution. In constant pressure MD simulations, we observed a clear trend of change of the phosphorus Q^n distribution as a function of cooling rate during simulated glass formation. With decreasing cooling rate, there is an increase of Q^0 and Q^1 species of phosphorus.

The increase in molar volume with the level of SrO/CaO substitution and the lower field strength of strontium as compared to calcium result in a weaker Si−O network and easier diffusion pathways for cation/water exchange that will lead to a higher dissolution rate of strontium substituted glasses. Except for the beneficial effect of strontium ions on bone cell growth, the increase of dissolution rate will also lead to an increase of bioactivity of strontium containing bioactive glasses that can find a number of biomedical applications.

■ ASSOCIATED CONTENT

Supporting Information. Size and cooling rate effect on the cation coordination number, structure factors, and P and Si Q^n distributions. This material is available free of charge via the Internet at http://pubs.acs.org/.

■ AUTHOR INFORMATION

Corresponding Author

*To whom correspondence should be addressed. E-mail: jincheng.du@unt.edu. Phone: 1-940-369-8184.

■ ACKNOWLEDGMENT

This work was supported by the U.S. National Science Foundation (NSF) (DMR-0907593). We appreciate Prof. Robert J. Newport and Dr. Victoria FitzGerald for providing the experimental neutron structure factor data.

■ REFERENCES

(1) Hench, L. L.; Polak, J. M. *Science* **2002**, *295*, 1014 + 1016–1017.
(2) Hench, L. L. *J. Mater. Sci. Mater. Med.* **2006**, *17*, 967–78.
(3) Renaudin, G.; Laquerriere, P.; Filinchuk, Y.; Jallot, E.; Nedelec, J. M. *J. Mater. Chem.* **2008**, *18*, 3593–3600.
(4) Xue, W.; Moore, J. L.; Hosick, H. L.; Bose, S.; Bandyopadhyay, A.; Lu, W. W.; Cheung, K. M. C.; Luk, K. D. K. *J. Biomed. Mater. Res., Part A* **2006**, *79*, 804–814.
(5) Tian, M.; Chen, F.; Song, W.; Song, Y.; Chen, Y.; Wan, C.; Yu, X.; Zhang, X. *J. Mater. Sci. Mater. Med.* **2009**, *20*, 1505–1512.
(6) O'Donnell, M. D.; Fredholm, Y.; de Rouffignac, A.; Hill, R. G. *Acta Biomater.* **2008**, *4*, 1455–1464.
(7) Boyd, D.; Murphy, S.; Towler, M. R.; Wren, A. W.; Hayakawa, S. *J. Non Cryst. Solids* **2009**, *355*, 2285–2288.
(8) Murphy, S.; Boyd, D.; Moane, S.; Bennett, M. *J. Mater. Sci. Mater. Med.* **2009**, *20*, 2207–2214.
(9) Lao, J.; Nedelec, J. M.; Jallot, E. *J. Mater. Chem.* **2009**, *19*, 2940–9.
(10) Abou Neel, E. A.; Chrzanowski, W.; Pickup, D. M.; O'Dell, L. A.; Mordan, N. J.; Newport, R. J.; Smith, M. E.; Knowles, J. C. *J. R. Soc. Interface* **2009**, *6*, 435–446.
(11) O'Donnell, M. D.; R, G. H. *Acta Biomater.* **2010**, *6*, 2383.
(12) FitzGerald, V.; Pickup, D. M.; Greenspan, D.; Sarkar, G.; Fitzgerald, J. J.; Wetherall, K. M.; Moss, R. M.; Jones, J. R.; Newport, R. J. *Adv. Funct. Mater.* **2007**, *17*, 3746–3753.
(13) Tilocca, A.; Cormack, A. N.; de Leeuw, N. H. *Faraday Discuss.* **2007**, *136*, 45–55.
(14) Tilocca, A.; de Leeuw, N. H. *J. Phys. Chem. B* **2006**, *110*, 25810–16.
(15) Tilocca, A.; de Leeuw, N. H.; Cormack, A. N. *Phys. Rev. B* **2006**, *73*, 104209–1.
(16) Tilocca, A. *J. Chem. Phys.* **2008**, *129*, 084504–1.
(17) Tilocca, A.; Cormack, A. N. *J. Phys. Chem. B* **2007**, *111*, 14256–64.
(18) Tilocca, A. *Phys. Rev. B* **2007**, *76*, 224202–1.

(19) Pedone, A.; Malavasi, G.; Menziani, M. C. *J. Phys. Chem. C* **2009**, *113*, 15723–15730.
(20) Du, J.; Cormack, A. N. *J. Non Cryst. Solids* **2005**, *351*, 956–956.
(21) Du, J.; Cormack, A. N. *J. Am. Ceram. Soc.* **2005**, *88*, 2532–2539.
(22) Du, J.; Corrales, L. R. *J. Non Cryst. Solids* **2006**, *352*, 3255–3269.
(23) Tilocca, A.; Cormack, A. N.; de Leeuw, N. H. *Chem. Mater.* **2007**, *19*, 95–103.
(24) Cormack, A. N.; Zeitler, T. R. *J. Cryst. Growth* **2006**, *294*, 96–102.
(25) Tilocca, A.; Cormack, A. N. *J. Phys. Chem. C* **2008**, *112*, 11936–11945.
(26) Leshchenko, P. P.; Shevchenko, A. V.; Lykova, L. N.; Kovba, L. M.; Ippolitova, E. A. *Inorg. Mater.* **1982**, *18*, 1013–16.
(27) Nishi, F. *Acta Crystallogr., Sect. C* **1997**, *C53*, 534–6.
(28) Catti, M.; Gazzoni, G. *Acta Crystallogr., Sect. B* **1983**, *B39*, 679–84.
(29) Smith, W.; Forester, T. R. *J. Mol. Graph.* **1996**, *14*, 136–141.
(30) Wright, A. C.; Wagner, C. N. J. *J. Non-Cryst. Solids* **1988**, *106*, 85–88.
(31) Sears, V. *Neutron News* **1992**, *3*, 26.
(32) Loucks, R. J.; Mauro, J. C.; Tandia, A.; Timofeev, N. T. *J. Am. Ceram. Soc.* **2007**, *90*, 4020–4022.
(33) Nelson, C.; Tallant, D. R. *Phys. Chem. Glasses* **1984**, *25*, 31–38.
(34) Grussaute, H.; Montagne, L.; Palavit, G.; Bernard, J. L. *J. Non-Cryst. Solids* **2000**, *263−264*, 312–317.
(35) Dupree, R.; Holland, D.; Mortuza, M. G. *Phys. Chem. Glasses* **1988**, *29*, 18–21.
(36) Du, J.; Corrales, L. R. *J. Chem. Phys.* **2006**, *125*, 114702–1.
(37) Kohara, S.; Suzuya, K. *Nucl. Instrum. Meth. Phys. Res., Sect. B* **2003**, *199*, 23–28.
(38) Tilocca, A. *Proc. R. Soc. Londone, Ser. A* **2009**, *465*, 1003–1027.
(39) Pedone, A. *J. Phys. Chem. C* **2009**, *113*, 20773–84.
(40) Tilocca, A.; De Leeuw, N. H. *J. Mater. Chem.* **2006**, *16*, 1950–1955.
(41) Angelopoulou, A.; Montouillout, V.; Massiot, D.; Kordas, G. *J. Non Cryst. Solids* **2008**, *354*, 333–40.
(42) Pedone, A.; Charpentier, T.; Malavasi, G.; Menziani, M. C. *Chem. Mater.* **2010**, *22*, 5644–5652.
(43) Cerruti, M.; Magnacca, G.; Bolis, V.; Morterra, C. *J. Mater. Chem.* **2003**, *13*, 1279–1286.
(44) Wright, A. C.; Clare, A. G.; Bachra, B.; Sinclair, R. N.; Hannon, A. C.; Vessal, B. . In *Proceedings of the Symposium on The Structural Chemistry of Silicates*; July 22−July 24, 1991; American Crystallographic Association: Toledo, OH, 1991; Vol. 27, pp 239−254.
(45) Cerruti, M.; Bianchi, C. L.; Bonino, F.; Damin, A.; Perardi, A.; Morterra, C. *J Phys Chem B* **2005**, *109*, 14496–14505.
(46) Eckersley, M. C.; Gaskell, P. H.; Barnes, A. C.; Chieux, P. *J. Non-Cryst. Solids* **1988**, *106*, 132–136.
(47) McKeown, D. A.; Kot, W. K.; Pegg, I. L. *J. Non Cryst. Solids* **2003**, *317*, 290–300.
(48) Johnson, J. A.; Urquidi, J.; Holland, D.; Johnson, C. E.; Appelyard, P. G. *J. Non Cryst. Solids* **2007**, *353*, 4084–92.
(49) Shannon, R. D. *Acta Crystallogr., Sect. A* **1976**, *A32*, 751–67.
(50) Mead, R. N.; Mountjoy, G. *J. Phys. Chem. B* **2006**, *110*, 14273–14278.
(51) Tilocca, A. *J. Mater. Chem.* **2010**, *20*, 6848–6858.
(52) Creux, S.; Bouchet-Fabre, B.; Gaskell, P. H. *J. Non-Cryst. Solids* **1995**, *192−193*, 360–363.
(53) Andersson, O. H.; Sodergard, A. *J. Non Cryst. Solids* **1999**, *246*, 9–15.
(54) Waclawska, I.; Stoch, L. *J. Therm. Anal. Calorim.* **2001**, *65*, 141–146.
(55) Hill, R. *J Mater. Sci. Lett.* **1996**, *15*, 1122.